Irradiance sensor implementation using commercial bifacial PV modules

Rodrigo P. Maruyama[1], Alex Renan A. Manito[1], André Ricardo Mocelin[1], Givaldo dos Reis[1], Teddy A. F. Meléndez[1], Marcelo P. Almeida[1], Roberto Zilles[1]

[1]*Institute of Energy and Environment, São Paulo (Brazil)*

Abstract

The number of photovoltaic systems has grown exponentially in recent years in Brazil and worldwide, largely due to the quality and reliability of the technology. To ensure that a system is operating under the designed conditions, it is necessary to evaluate its performance, which basically uses the energy incident on the generator and the energy injected into the electrical grid. However, systems using bifacial photovoltaic modules present significant complexity when quantifying the total energy incident on the generator plane, since the rear-side irradiance component is influenced by several external factors such as albedo, generator height above the ground, and surrounding surface composition. Therefore, characterizing the irradiance incident on the back of bifacial photovoltaic modules is essential to accurately quantify the bifacial gain and evaluate the performance of these systems. Since point irradiance sensors such as pyranometers or reference cells do not "see" the entire generator plane, they can introduce measurement biases that lead to inaccurate estimations of the total irradiance. This paper describes the design and construction of a reference photovoltaic module, specially designed as a practical alternative to conventional radiation sensors. The proposed reference module offers a low-cost and easy-to-integrate solution, contributing to improving performance studies and modeling of bifacial systems.

Keywords: solar, photovoltaic, bifacial reference module, monitoring, sensor, irradiance

1. Introduction

In 2024, photovoltaic (PV) technology reached a major milestone by supplying about 10.8% of the total global electricity demand (IEA, 2025). This achievement highlights the growing role of solar energy as one of the main pillars of the global power system. The expansion has been fueled by a combination of rapid technological improvements, large-scale manufacturing growth, and continued cost reductions that have made PV the most competitive source of new electricity generation in most regions. The number of connected systems in Brazil and around the world is growing significantly. In Brazil, there are already almost 3.8 million systems connected to the electric grid, totaling almost 60 GWp of installed power (ABSOLAR, 2025), while worldwide the installed capacity has already surpassed the 2.2 TWp mark (IEA, 2025).

One of the defining features of 2024 is the widespread adoption of bifacial PV modules. It is estimated that more than 75% of all modules manufactured during the year were bifacial, up from about 50% in 2023 (IEA, 2025). This transition represents a technological shift toward higher efficiency and better energy yields, particularly in utility-scale applications. However, challenges remain in accurately modeling and simulating the rear-side irradiance contribution due to its complexity, which continues to limit the precision of bifacial performance assessments.

To ensure the reliability of the systems and consequently guarantee financial return, the energy projected for generation must be achieved and maintained. To assess whether the system is performing as expected, it is necessary to evaluate the system's performance using the solar energy reaching the generator (photovoltaic module), the energy injected into the electric grid, and the nominal power of the PV system.

This work presents the applicability of modified bifacial reference photovoltaic modules for measuring the irradiance incident on bifacial modules operating under real outdoor conditions. A total of six bifacial modules were prepared and calibrated, three of them were modified to measure three irradiance components (G_{front}, G_{rear}, and G_{total}), while the other three *Unmodified modules* were used for independent measurements of each component.

The study utilized the infrastructure of two photovoltaic systems for data acquisition. One experiment is a rooftop system, while the other is a fixed-tilt ground-mounted system.

The rooftop experiment evaluates the performance of the modified reference module by comparing its measured

10.18086/swc.2025.03.36 Available at http://proceedings.ises.org

irradiances with those obtained from the unmodified reference modules. The fixed-tilt system experiment investigates the irradiance measured at two vertical positions within the array (top and bottom strings) to: (i) quantify the difference in rear-side irradiance due to system geometry and shading effects, and (ii) provide an effective irradiance reference on the array plane for system performance evaluation.

2. Literature review

The origin of bifacial photovoltaic technology dates to 1966, when Hiroshi Mori patented a semiconductor device with p–n junctions on both sides, allowing light absorption from either face, thus resulting in greater energy conversion efficiency (Mori, 1966).

Decades later, between 1983 and 1989, the Instituto de Energía Solar (IES-UPM) and ISOFOTON in Spain achieved the first industrial production and modelling of bifacial modules. Led by Antonio Luque and Eduardo Lorenzo, the group introduced the view-factor concept to estimate rear-side irradiance and validated it experimentally in a 40 kW bifacial field with less than 3 % deviation between measured and modelled values. They also developed the concepts of albedo maps, sky maps, and figure of merit for energy-gain assessment. Although ISOFOTON ceased production in 1989, this pioneering work established the theoretical basis for future models (Lorenzo, 2021). After a long hiatus, bifacial research re-emerged in the 1990s and expanded during the 2000s with new 3-D models and field experiments. In 2012, PVsyst incorporated the view-factor approach.

Between 2006 and 2010, Martínez-Moreno et al. (2012) reported the characterization of about 200 MW of commercial PV plants in Spain. Their work addressed uncertainty analysis, reference module calibration, and measurement procedures for array power verification.

In Brazil, the publication of NBR 16274:2014 marked a significant milestone for the national photovoltaic market. The standard established the first systematic framework for evaluating the performance of grid-connected PV systems in the country. Its development was primarily guided by two key references: the work of Martínez-Moreno et al. (2011), which provided experimental methods for testing large-scale PV systems, and the dissertation by Almeida (2012b), which contributed methodological procedures for on-site evaluation of Brazilian PV installations. However, this standard did not include parameters related to rear-side irradiance or bifacial energy gain, reflecting the predominance of monofacial technology at that time.

In 2019, the *IEC TS 60904-1-2:2019* marked the first official step toward standardizing the measurement of bifacial photovoltaic devices. This technical specification established the procedures for determining the current–voltage characteristics of bifacial modules under controlled illumination and introduced the key concept of effective irradiance, expressed as

$$G_{\text{eff}} = G_{\text{front}} + \alpha\, G_{\text{rear}} \qquad (eq.1)$$

where α is the bifaciality coefficient of the module, representing the relative response of the rear side compared to the front side. The document also defined the calculation of bifacial gain, given by

$$G_{\text{gain}}(\%) = \frac{G_{\text{eff}} - G_{\text{front}}}{G_{\text{front}}} \times 100 \qquad (eq.2)$$

which provides the first formal quantitative framework for comparing bifacial and monofacial devices based on irradiance contribution and electrical performance.

In 2021, two key revisions were published: IEC 61215-2:2021 and IEC 61724-1/-2:2021. The IEC 61215-2:2021 introduced several specific tests for bifacial modules, while the IEC 61724 series introduced the concept of bifaciality into the calculation of the Performance Ratio (PR). The annual equivalent performance ratio for bifacial systems ($PR'_{\text{annual-eq,bi}}$) is defined as:

$$PR'_{\text{annual-eq,bi}} = \frac{\sum_k P_{\text{out},k}\, \tau_k}{\sum_k \left(\frac{C_{k,\text{annual}}\, P_0\, G_{i,k}\, BIF_k\, \tau_k}{G_{i,\text{ref}}}\right)} \qquad (eq.3)$$

where $P_{\text{out},k}$ is the instantaneous output power, τ_k the time interval, $C_{k,\text{annual}}$ the correction coefficient, P_0 the nominal power, $G_{i,k}$ the plane-of-array irradiance, BIF_k the bifaciality factor, and $G_{i,\text{ref}} = 1000\ \text{W/m}^2$ the reference irradiance.

The bifaciality factor BIF accounts for the irradiance contribution of both faces of the module and is defined as:

$$BIF = 1 + \phi_{p,\max}\,\rho_i \qquad (eq. 4)$$

where $\phi_{p,\max}$ is the maximum-power bifaciality coefficient (ratio between rear and front $P_{\max}$ at STC, and ρ_i is the in-plane rear-to-front irradiance ratio.

By substituting Equation (2) into Equation (1), the expanded annual equivalent $PR'_{\text{annual-eq,bi}}$ becomes:

$$PR'_{\text{annual-eq,bi}} = \frac{\sum_k P_{\text{out},k}\,\tau_k}{\sum_k \left(\frac{C_{k,\text{annual}}\,P_0\,G_{i,k}\,[1 + \phi_{p,\max}\,\rho_{i,k}]\,\tau_k}{1000}\right)} \qquad (eq. 5)$$

This formulation incorporates the contribution of rear-side irradiance (ρ_i).

The research on rear-side irradiance measurement in bifacial photovoltaic (PV) systems (Gostein et al. (2020), Polo et al. (2021), Braid et al. (2022), Riedel-Lyngskær et al. (2022), and Babal (2022)) can be grouped into three main categories:

1. Comparison of sensor technologies, which focuses on evaluating the accuracy of different irradiance sensors;
2. methodological frameworks and measurement strategies, which propose procedures and uncertainty models for bifacial monitoring;
3. development and field validation of reference modules, which demonstrate practical implementations of bifacial reference devices.

Studies in this category focused on assessing how various irradiance sensors capture the optical conditions of bifacial arrays.

Braid et al. (2022) compared pyranometers and bifacial reference modules across a 175.6 MW DC single-axis tracking plant, showing that pyranometers overestimated effective irradiance by 2.5–4.5%, resulting in a deviation of ~3.9% in capacity test results. Riedel-Lyngskær et al. (2022) validated bifacial reference modules calibrated under IEC TS 60904-1-2, reporting mean absolute errors below 9% for rear POA irradiance and 4% for effective irradiance when compared to reference cells. Complementarily, Babal (2022) quantified the influence of sensor type and mounting position, finding that sensors placed at 40–60% of the panel height provided the lowest combined uncertainty due to better spectral matching.

Gostein et al. (2020) presented one of the first comprehensive methodological reviews of rear-irradiance measurement approaches for bifacial PV systems. Their work analyzed the trade-offs between direct and model-based measurement techniques, uncertainty propagation, and instrumentation cost. Experimental case studies revealed that omitting rear-side measurements can introduce more than 10% uncertainty in performance assessment, while direct measurement substantially improves the accuracy of energy-yield estimation.

Polo et al. (2021) proposed a straightforward method for converting commercial bifacial modules into calibrated sensors that can measure both front and rear irradiance simultaneously. Their rooftop experiments revealed high rear-irradiance variability caused by shading and edge effects, underscoring the need for representative sensor placement. Similarly, Riedel-Lyngskær et al. (2022) demonstrated that calibrated bifacial reference panels could reduce the uncertainty of bifacial performance-ratio calculations by approximately ±1.5%.

This work advances the study of rear-side irradiance measurement by combining experimental assessment and calibration analysis under real operating conditions. The study begins with an evaluation of the behavior of bifacial PV modules used as irradiance sensors, comparing full-size reference modules with modified ones specifically designed for simultaneous front- and rear-side measurements. Additionally, it includes an examination of the uncertainty achieved by the laboratory in developing and calibrating bifacial reference modules, as well as establishing traceability in accordance with *IEC 60904-4* and *IEC 61724-1*.

The research also provides a quantitative analysis of bifacial gain in a real fixed-tilt PV system, using calibrated reference modules to determine effective irradiance and energy yield. Moreover, it explores the variation in rear-side irradiance between strings positioned at different locations within the same array, highlighting the effects of geometry and shading on overall system performance. Together, these investigations contribute experimental evidence that strengthens the methodological foundation for accurate irradiance measurement and performance evaluation of bifacial PV systems.

3. Materials and methods

3.1. Laboratory Infrastructure

All calibration procedures and reference module characterizations were carried out in a metrological laboratory accredited by the Brazilian National Institute of Metrology, Quality and Technology (INMETRO) and a signatory to the International Laboratory Accreditation Cooperation - Mutual Recognition Arrangement (ILAC-MRA). The laboratory operates in accordance with the requirements of ISO 17025, ensuring full traceability of measurements and high metrological reliability. It is equipped with a Class A+A+A+ solar simulator, compliant with IEC 60904-9, which allows for precise current–voltage characterization of photovoltaic devices under controlled irradiance, spectrum, and spatial uniformity conditions. This infrastructure enables the calibration of reference modules and the evaluation of their performance with high accuracy, supporting the experimental validation of the irradiance measurements used in this study.

3.2. Bifacial PV module

The photovoltaic modules used in this study are bifacial monocrystalline silicon devices manufactured by a Tier-1 producer. Each module has a rated maximum power (P_{max}) of 545 W under standard test conditions (STC) and are certified in accordance with IEC 61215 (Design Qualification and Type Approval) and IEC 61730 (Photovoltaic Module Safety Qualification). The modules feature 144(6x24) half-cut bifacial PERC cells encapsulated in a glass-glass structure and include a 12-year product warranty and a 30-year linear power output warranty, with an annual degradation rate of approximately 0.45 % per year (2% in the first year), guaranteeing at least 85 % of the initial power after 30 years of operation. According to the product datasheet, the module has the specifications described in Table 1.

Table 1: Commercial bifacial PV module specifications.

Electrical specifications	Mechanical specifications
Pmax: 545 W;	Dimension (L×W×H): 2,278×1,134×30 mm;
Voc: 49,75 V;	Weight: 31.8 kg;
Isc: 13,93 A;	Front glass: 2 mm;
Maximum System Voltage: 1500 V DC;	Rear glass: 2 mm;
Temp. coef. of power (γ): –0.35%/°C;	Maximum Static Load, Front: 5400 Pa;
Efficiency: 21,1%;	Maximum Static Load, Rear: 2400 Pa;
Bifaciality factor: 70% ± 10%;	Operating Temperature: –40 °C to +85 °C.

3.3. Reference module implementation

The reference photovoltaic module used in this study complies with Clause 4.3(a) of IEC 60904-2:2023, which specifies additional requirements for reference modules regarding bypass diodes. According to the second paragraph of this clause, when a reference module is intended to be matched to the module under test, the number, type, and connection of bypass diodes shall be identical to those present in the module under test.

In the present work, the selected reference module is identical to the module used in the photovoltaic system under study, being of the same model and electrical configuration, including the bypass-diode arrangement. This ensures fully equivalent electrical behavior under partial-irradiance or mismatch conditions, enabling a direct and accurate comparison of the short-circuit current and I–V characteristics between the two devices. Therefore, the selected reference module fully satisfies the requirements of Clause 4.3(a) of IEC 60904-2:2023.

Two types of reference modules were employed in the experiments: modified and unmodified. Both are based on the same bifacial module model described previously, but they differ in their electrical configuration and surface treatment.

The *Modified module* had the three bypass diodes originally present in the junction box. They were removed, and conductors were connected to the positive and negative terminals to enable the electrical connection to an external shunt resistor for voltage measurement. Additionally, a vinyl film was applied to specific regions of the module surface to isolate the measurement of the irradiance components: i) on the front side, right half of the module (Figure 1b) to measure rear-side irradiance, and ii) on the rear side, left half (Figure 1b) to measure front-side irradiance.

The *Unmodified module* retained its original electrical configuration, with the three bypass diodes intact. Only the vinyl film was applied to control the irradiance incidence on each surface: i) on the front side to measure rear-side irradiance, and ii) on the rear side to measure front-side irradiance.

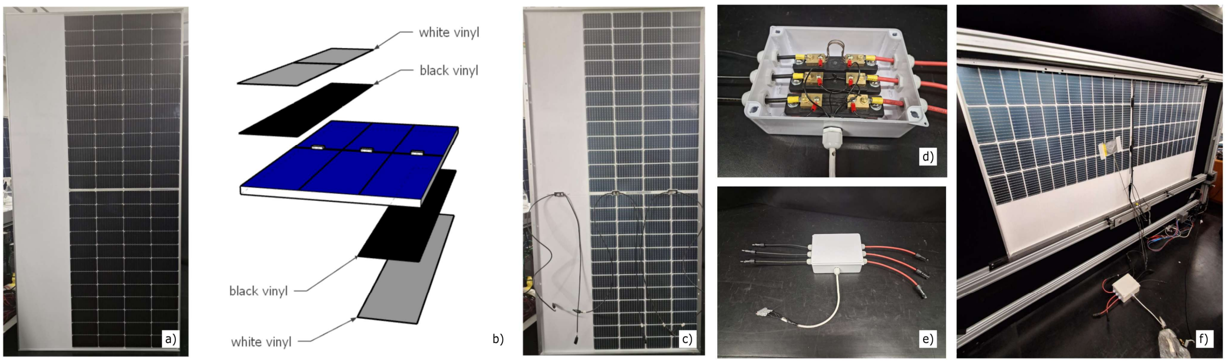

Figure 1: a) Front side of the modified bifacial PV module. b) Scheme of vinyl order and location of application. c) Rear side of the modified bifacial PV module. d) Shunt resistor box inside view. e) Shunt resistor box external view. f) Calibration of the reference bifacial PV module.

3.6. Shunt resistor

The built-in shunt resistor was selected in accordance with the requirements of IEC 60904-2: Photovoltaic Devices – Part 2: Requirements for Reference Solar Devices, which specifies that the resistor must be low enough to ensure operation of the reference device close to short-circuit conditions. According to section 4.4 of the standard, this condition is satisfied when the resistance R_{CAL} meets the criterion:

$$R_{CAL} < \frac{0.2 \times V_{OC}}{I_{SC}} \qquad (eq. 6)$$

where V_{OC} is the open-circuit voltage and I_{SC} is the short-circuit current of the reference device under the desired reference conditions.

For the reference module used in this study, the measured parameters were $V_{OC} = 49.75$ V and $I_{SC} = 13.93$ A, resulting in a maximum allowable resistance of $R_{CAL,max} = 0.714\ \Omega$.

3.7. Calibration procedure

The calibration of the reference module was performed by an ILAC-MRA signatory laboratory, ensuring international traceability and compliance with recognized metrological standards. The procedure was carried out using a PASAN Class A+A+A+ solar simulator, which fulfills the spectral match, irradiance non-uniformity, and temporal instability requirements specified in IEC 60904-9.

In accordance with Clause 7.1 of IEC 60904-2, the calibration was executed following a documented and traceable procedure in accordance with IEC 60904-4. All instruments involved in the measurement process maintain an unbroken traceability chain to national and international standards. The calibration laboratory also maintains a documented uncertainty analysis, as well as interlaboratory comparison results, ensuring the reliability and consistency of the calibration data obtained for the reference device.

3.8. Uncertainty analysis

The combined and expanded uncertainties of the calibration procedure were determined according to the statistical framework described in ISO/IEC Guide 98-3 (GUM) and required by Clause 5 of IEC 60904-4. The approach adopted in this work follows the Guide to the Expression of Uncertainty in Measurement (GUM) (Baratto, A.C. et al., 2008)

According to the GUM, measurement uncertainty is defined as a non-negative parameter that characterizes the dispersion of values attributed to a measurand based on available information and represents the degree of confidence associated with the estimate of an essentially unique true value of the measurand.

The calibration results were satisfactory, yielding a combined standard uncertainty of 1.562523236 % for the reference module. According to the *Guide to the Expression of Uncertainty in Measurement* (Baratto, A.C. et al., 2008, Section 7.2.6 and 7.2.7), all intermediate calculations shall be performed using the full numerical precision, and only the final reported value shall be rounded. Following this recommendation, the expanded uncertainty is expressed with no more than two significant digits, resulting in a final reported uncertainty of 1.56 %.

At an irradiance level of 1000 W/m², this corresponds to 15.6 W/m².

The combined standard uncertainty, calculated from the independent standard uncertainties of the front- and rear-side irradiance measurements, was obtained according to the root-sum-of-squares method:

$$u_c = \sqrt{u_{G\_front}^2 + u_{G\_rear}^2} \qquad (eq.7)$$

considering $U_{G\_front} = U_{G\_rear} = 1.562523236$ %, the resulting combined uncertainty is $U_{G\_total} = 2.21097\%$. Therefore, the total combined uncertainty for G_{total} is reported as 2.21 %, in accordance with the GUM's rounding guidelines.

3.4. Rooftop-mounted experiment

The Rooftop-mounted experiment consists of five PV calibrated modules installed on a flat rooftop. One of the modules, intentionally disconnected and marked with a red "X," was used to mitigate edge effects on irradiance distribution. Among the remaining modules, one specially modified and calibrated reference module measures the front, rear, and total irradiance components (G_front, G_rear, G_total). Three additional calibrated reference modules independently measure each of these quantities to provide redundancy and validation of the *Modified module's* performance. The rooftop array is oriented with an azimuth of 30° west as shown in Figure 2.

3.5. Ground-mounted experiment

The second system consists of a ground-mounted PV array composed of three strings with eight bifacial PV modules each (545 W per module), connected to a 20 kW three-phase inverter. Two of these modules were also modified and calibrated to measure the front and rear irradiance components within the generator plane. This configuration enables the evaluation of vertical irradiance gradients and geometric effects between strings. The system is oriented with an azimuth of 16° west as shown in Figure 3.

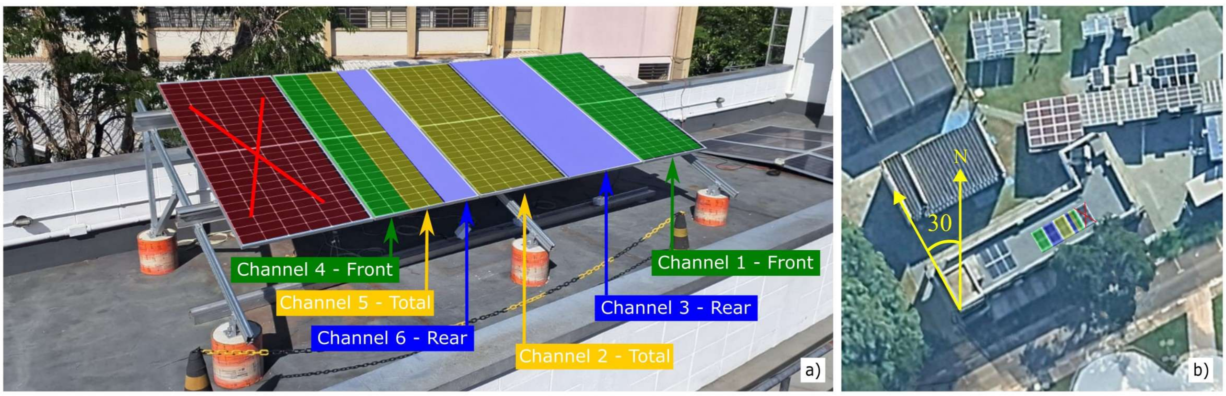

Figure 2: a) Rooftop-mounted PV system experiment consisting of five modules. One module (marked with red "X") disconnected is used to decrease border effect, one modified and calibrated module to measure G_front, G_rear and G_total, one calibrated module to measure the G_front, one calibrated module to measure the G_rear and one calibrated module to measure the G_total irradiance. b) Orientation of the rooftop PV system experiment, with an azimuth of 30° west.

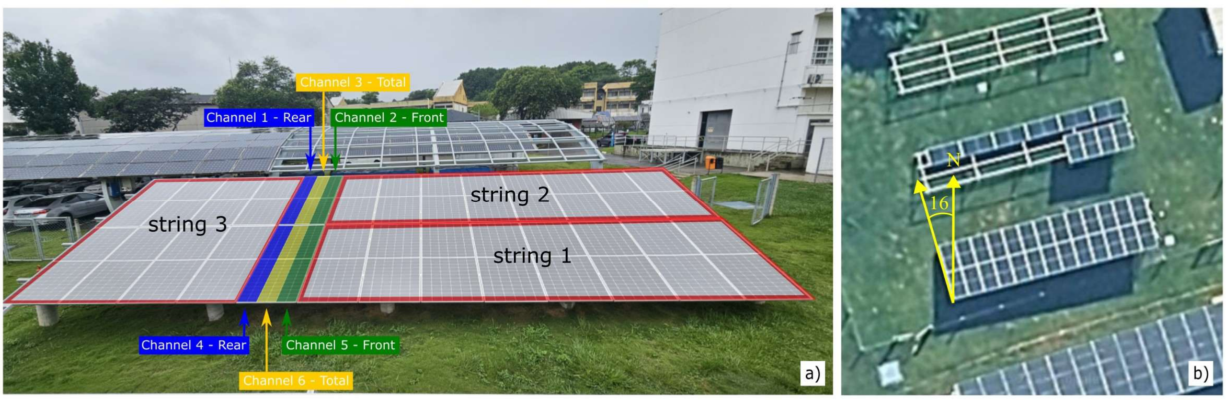

Figure 3: a) The ground-mounted PV system experiment consisting of three strings of 8 bifacial PV modules (545 W each) connected to a 20 kW three-phase inverter, and includes 2 modified and calibrated modules. b) The figure shows the PV system azimuth in 16° west.

4. Results and Discussion

The rooftop experiment successfully met one of its main objectives: to validate the use of a modified reference module for simultaneous front and rear irradiance measurements under the same conditions as the unmodified reference modules. However, due to edge effects and the system azimuth, the rear-side irradiance exhibited a measurable bias associated with these geometric characteristics. This behavior can be clearly observed in the irradiance profile of G_{rear} shown in Figure 5, as well as in the heatmap of Figure 6, where the highest irradiance values are concentrated in the morning for the *Modified module* and in the afternoon for the *Unmodified module*. These results highlight the influence of the module positioning within the array and indicate the need for further refinement of the experimental setup to minimize such positional effects in future analyses.

A statistical analysis was carried out on the irradiance data obtained from the *Unmodified* and *Modified reference modules* to verify their statistical agreement and validate the applicability of the *Modified module* in the ground-mounted experiment. Two complementary analyses were performed: one that plots the uncertainty margin of each measurement at every timestamp, and another that evaluates whether each measured value lies within its corresponding uncertainty range. Points displayed in green indicate that the values are statistically consistent (within the uncertainty interval), while points in red indicate that the measurements fall outside this range.

In the uncertainty comparison graphs, the expanded uncertainty (U) associated with each irradiance measurement was calculated according to:

$$U = k \cdot u_{\text{rel}} \cdot | G | \qquad (eq.8)$$

where u_{rel} is the relative standard uncertainty (1.563%), k = 2 is the coverage factor corresponding to a 95% confidence level, and |G| is the measured irradiance value in W/m². This formulation converts the dimensionless relative uncertainty into an absolute expanded uncertainty, which scales proportionally with the irradiance magnitude.

Using only u_{rel} would provide a relative ratio of uncertainty but not a physically meaningful interval expressed in irradiance units. By multiplying by the measured value |G|, the uncertainty becomes expressed in W/m², allowing a direct visual comparison between the uncertainty bands and the measured data. Furthermore, the multiplication by the coverage factor k ensures that the uncertainty interval corresponds to a 95% confidence level (Baratto, A.C. et al., 2008). The shaded regions shown in the uncertainty graphs represent the interval:

$$G \pm U \qquad (eq.9)$$

which defines, with approximately 95% confidence, the range within which the true irradiance value is expected to lie. In this study, the combined expanded uncertainty of 1.563% corresponds to ±15.63 W/m² at an irradiance level of 1000 W/m². This approach allows the visual identification of statistically significant deviations between the Unmodified and Modified reference module measurements. When the uncertainty bands overlap, the difference is considered statistically insignificant, whereas non-overlapping intervals (highlighted in red) indicate deviations exceeding the combined expanded uncertainty.

The overlap between the uncertainty intervals of both measurements was used as the criterion for statistical agreement, following the (eq. 10):

$$\text{Overlap}(t_i) = \neg\big((G_1 + U_1 < G_2 - U_2) \vee (G_2 + U_2 < G_1 - U_1)\big) \qquad (eq.10)$$

When the uncertainty intervals overlap, the difference is statistically insignificant (plotted in green). Conversely, non-overlapping intervals indicate statistically significant differences (plotted in red) (Figure 4).

The ground-mounted experiment successfully achieved its primary objective of evaluating the irradiance distribution across the generator plane and validating the use of modified reference modules under real operating conditions. The results showed consistent differences between the top and bottom strings, particularly in the rear-side irradiance values, which are consistent with the reference data reported by the IEA (2021, Figure 22), with the simulation results obtained using the System Advisor Model (SAM) for the studied configuration and in the heatmap in Figure 7. Unlike the rooftop-mounted experiment, the edge effect was mitigated due to the more central positioning of the reference modules within the array.

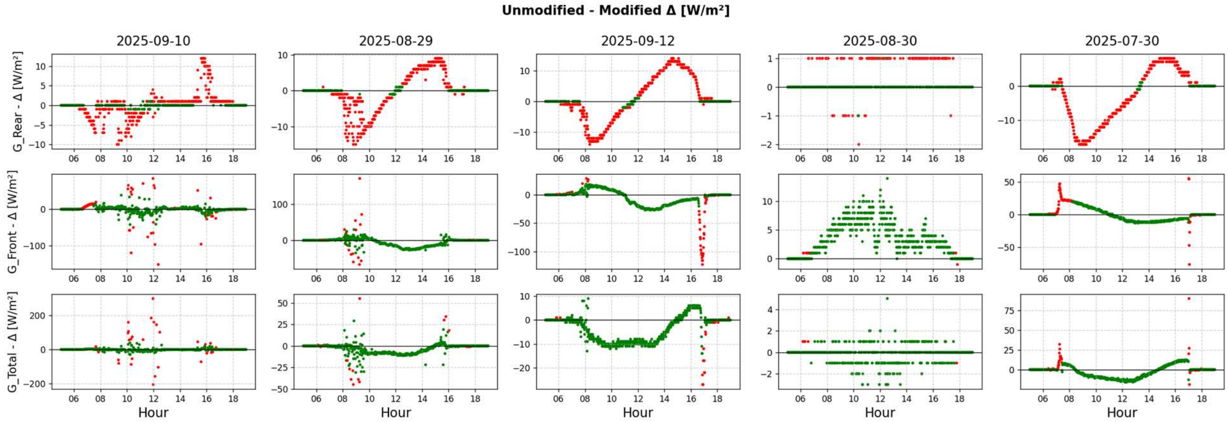

Figure 4: Uncertainty overlap analysis for irradiance measurements obtained from the rooftop experiment. Each row compares the instantaneous irradiance difference (Δ = Unmodified – Modified) between the two reference modules for the rear (G_rear), front (G_front), and total (G_total) components. Green points indicate that the expanded uncertainties of both measurements overlap, meaning the two readings agree statistically within the 95 % confidence interval (k = 2, u_rel = 1.56 %). Red points indicate no overlap, revealing significant differences beyond the combined uncertainty range.

Physically, these differences can be explained by the geometric configuration of the experimental setup. The rear-side bifacial reference modules were installed at different heights, where the lower module was positioned closer to the reflective plane (ground), with a clearance of 0.5 m, while the upper module was farther from both the ground and the surrounding reflective surfaces that contributed to diffuse irradiance. Since the radiation reflected from the ground behaves approximately as an isotropic local emission, the irradiance incident on the rear surface of the module follows an inverse of the square of the distance (r) from the reflective plane, expressed as:

$$I_{\text{rear}}(r) \propto \frac{1}{r^2} \qquad (eq. 11)$$

Where I_{rear} is the radiation intensity (W/m^2).

In the plots shown in Figure 7 (rows 10-12), irradiance values (x-axis) were compared to the corresponding power outputs (y-axis) for each time instant. This analysis enables the observation of the linear relationship between the two variables, particularly under clear-sky conditions. The slope of the regression line obtained for each dataset indicates the nominal power of the generator. However, only data within an appropriate irradiance range should be considered, and results must be corrected to Standard Test Conditions (STC) for meaningful interpretation (Almeida, 2012).

Although cell temperature is not yet monitored in the current setup, the inclusion of a temperature sensor is already planned and will allow the calculation of the generator's nominal power under standardized conditions. Furthermore, this additional measurement will enable long-term tracking of the modules' degradation rate, providing valuable insights into system performance over time.

The cumulative energy curves shown in Figure 7 (last row) illustrate the integrated irradiance over time for each measured component: front (E_{front}), rear (E_{rear}), and total ($E_{\text{total}} = E_{\text{rear}} + E_{\text{front}}$). From this data, the bifacial gain was calculated by combining (eq. 1) and (eq. 2) for $\alpha = 1$, resulting in the following expression:

$$Gain(\%) = \frac{E_{\text{rear}}(G_R)}{E_{\text{total}}(G_T)} \times 100 \qquad (eq. 12)$$

Where $E_{\text{rear}}(G_R)$ is the energy due to the rear irradiance, $E_{\text{total}}(G_T)$ is the energy due to the total irradiance.

The calculated bifacial gain values ranged from 2.79% to 5.65%, depending on the day and prevailing sky conditions. These results indicate that the rear-side contribution to the total irradiance varied with atmospheric conditions and system geometry, confirming the effective bifacial response of the array observed in Figure 8. However, manufacturers and several relevant studies report higher values, with possible increases of up to 35% for single-axis tracking systems, as highlighted by the IEA (2025).

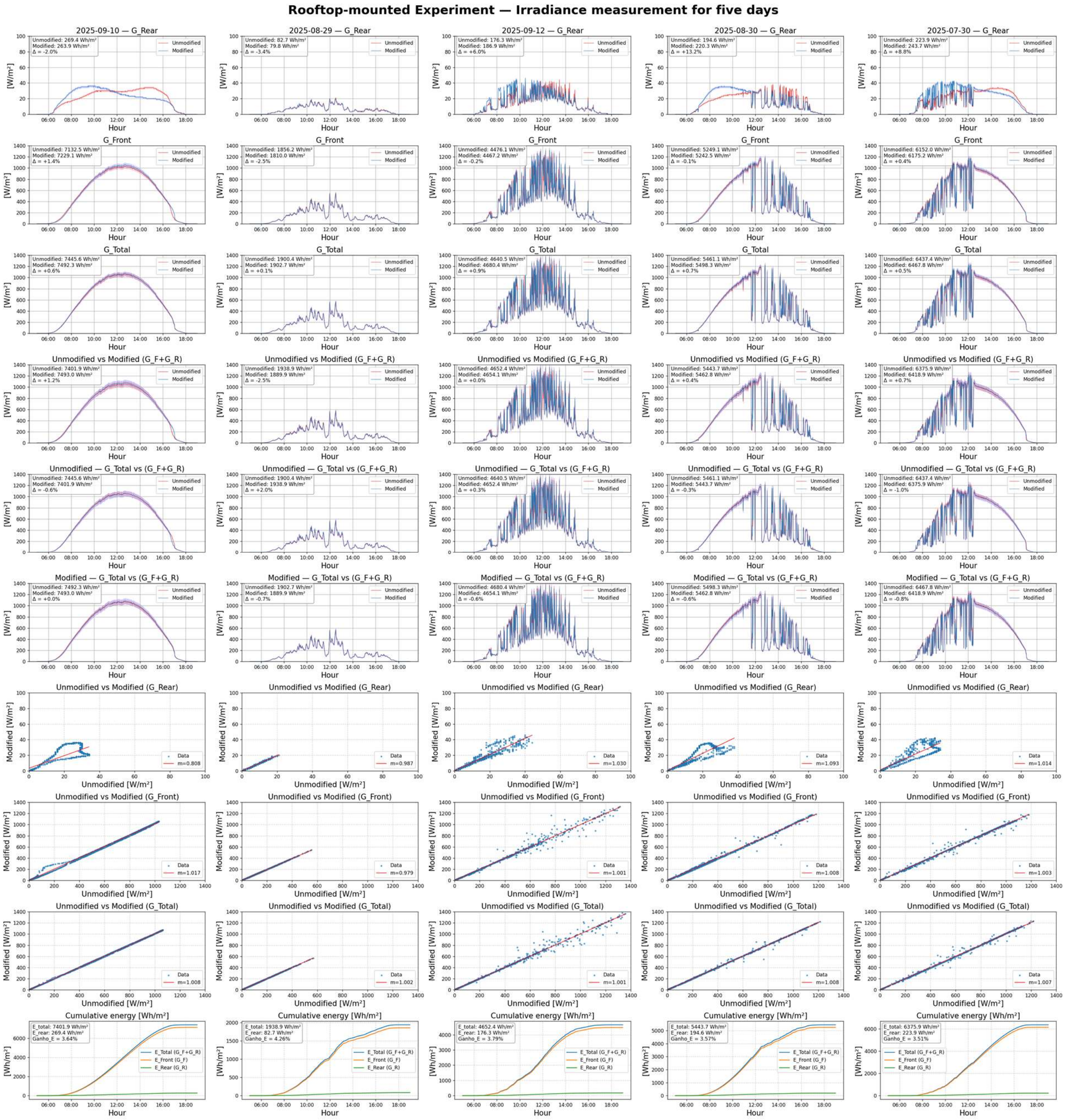

Figure 5: a) Rows 1–4: Measured front, rear, and total irradiance components (G_Front, G_Rear, G_Total) for each reference module pair, with smoothed and raw values over time. Row 5: Ratio between rear and front irradiance (G_Rear / G_Front), indicating the instantaneous bifacial gain during each day. Row 6: Comparison between top and bottom module sensors for front and rear sides, assessing the irradiance gradient along the array height. Rows 7–9: Linear regression between top and bottom irradiance values for front, rear, and total irradiance channels, with slope (m) and coefficient of determination (R^2) indicated on each plot. Last Row: Cumulative daily energy derived from irradiance integration for each configuration (front, rear, and bifacial total), including the computed bifacial gain percentage.

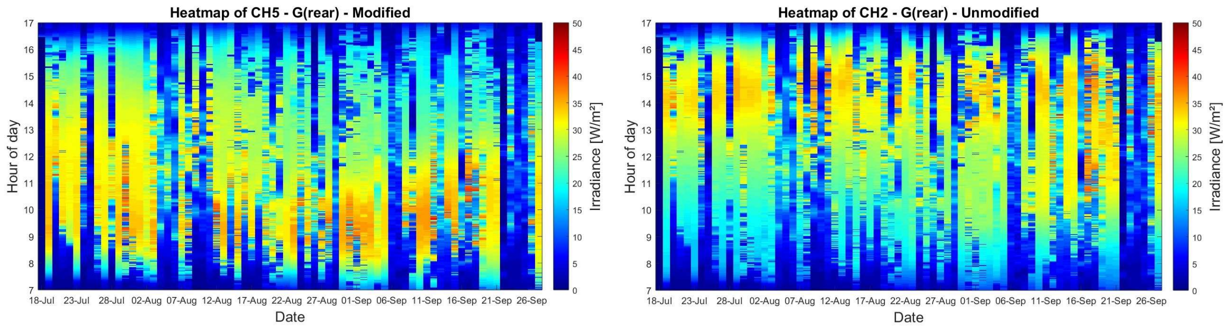

Figure 6: left) Heatmap of Rear Irradiance in [W/m^2] of the Modified reference module. right) Heatmap of Rear Irradiance in [W/m^2] of the Unmodified reference module. (20/07/25 – 26/09/25)

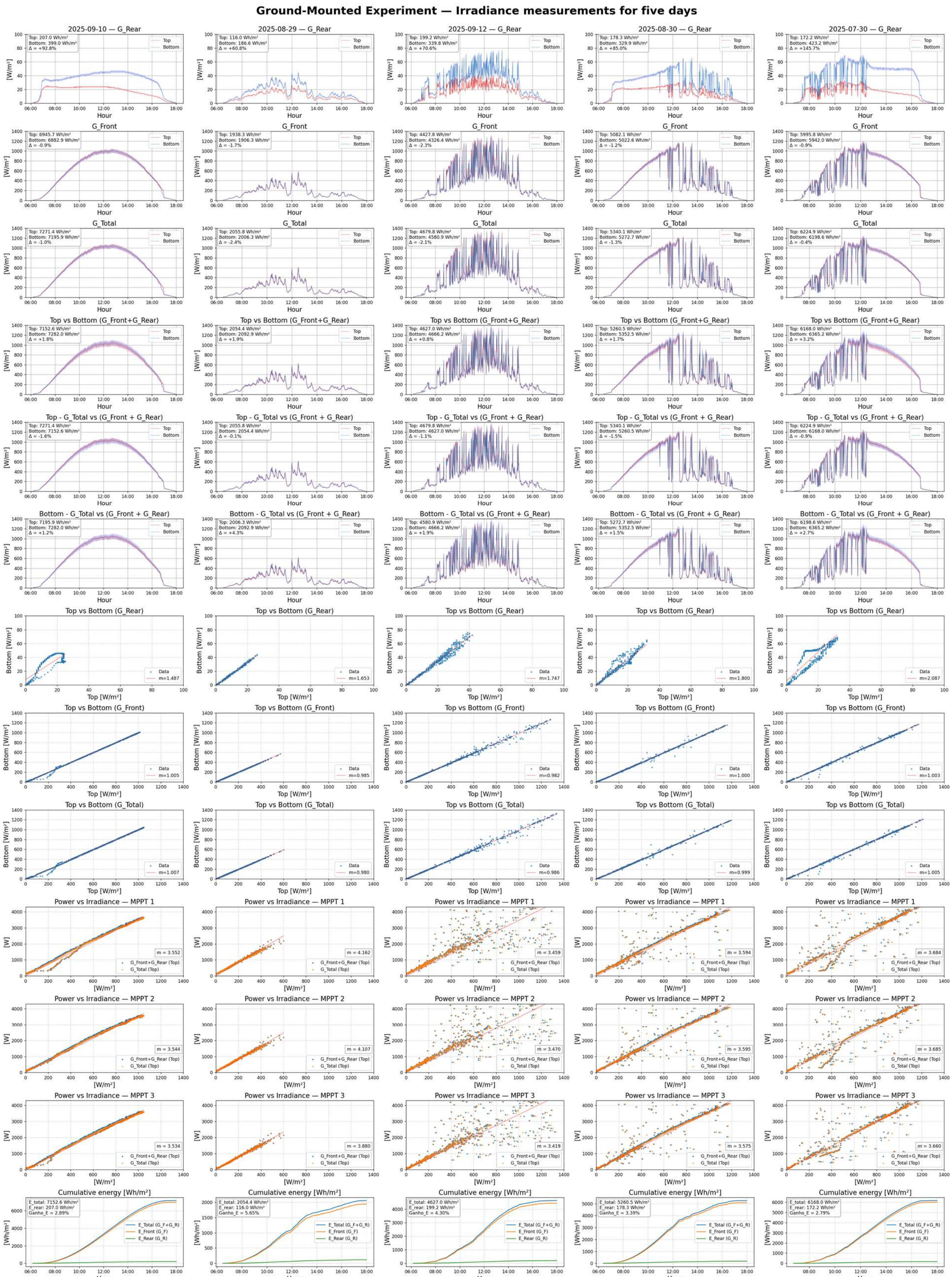

Figure 7: a) Rows 1–4: Measured front, rear, and total irradiance components (G_Front, G_Rear, G_Total) for each reference module pair, with smoothed and raw values over time. Row 5: Ratio between rear and front irradiance (G_Rear / G_Front), indicating the instantaneous bifacial gain during each day. Row 6: Comparison between top and bottom module sensors for front and rear sides, assessing the irradiance gradient along the array height. Rows 7–9: Linear regression between top and bottom irradiance values for front, rear, and total irradiance channels, with slope (m) and coefficient of determination (R^2) indicated on each plot. Rows 10–12: Correlation between DC power of each MPPT input (P_DC) and its corresponding irradiance, with regression line and calculated slope shown in the legend. Last Row (13): Cumulative daily energy derived from irradiance integration for each configuration (front, rear, and bifacial total), including the computed bifacial gain percentage.

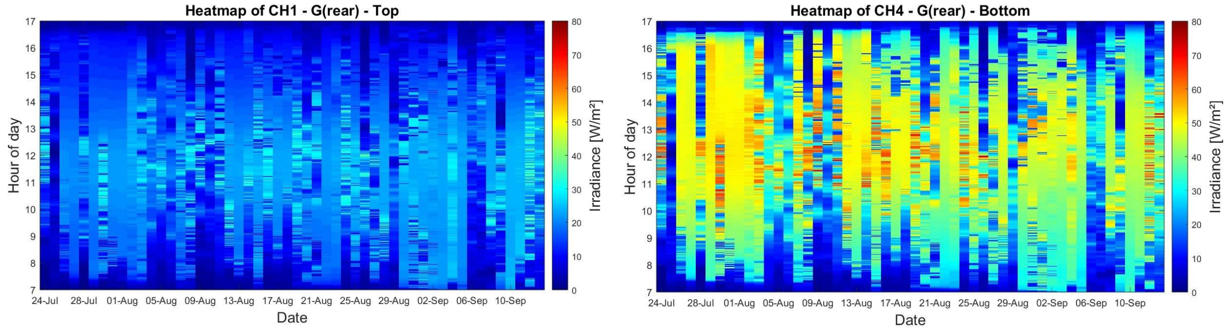

Figure 8: left) Heatmap of Rear Irradiance in [W/m^2] of the Top reference module. right) Heatmap of Rear Irradiance in [W/m^2] of the Bottom reference module. (24/07/25 – 13/09/25)

5. Conclusion

The modified reference modules demonstrate satisfactory statistical behavior, validating their use for measuring front, rear, and total irradiance. The rooftop experiment showed a rear-side irradiance bias due to azimuth orientation and edge effects, which confirms the predictions and opens opportunities for further studies, such as evaluating the influence of reference module positioning on edge effects. The application of the modified reference modules in the fixed-tilt real system showed consistency with previously published works and simulations performed using the SAM software, in which the rear-side irradiance on the lower module is higher than on the upper one due to its closer proximity to the plane where sunlight is reflected. The calculation of the generator's nominal power requires temperature correction to STC conditions, which is already planned and may be addressed in future work. Regarding the bifacial gain, it was modest, ranging from 2.79% to 5.65%. These positive results are attributed to the high quality of production and calibration of the reference modules, carried out by a specialized laboratory with low measurement uncertainty.

6. Acknowledgments

This research was supported by the National Council for Scientific and Technological Development (CNPq/MCTI, Brazil) under project No. 406711/2022-5, "Real-Sun Characterization of Bifacial Photovoltaic Modules and Generators: Establishing Foundations for Technology Consolidation in the Market." It was also carried out within the scope of the National Institute for Technological Development of Photovoltaic Solar Energy Applications (INCT-DAESF), CNPq/MCTI/Brazil, Process No. 408486/2024-4. We gratefully acknowledge the technicians and researchers of the Photovoltaic Systems Laboratory (LSF-IEE/USP) for their valuable support and the use of their infrastructure.

7. References

ABNT (2014) NBR 16274:2014 – Sistemas fotovoltaicos conectados à rede: Requisitos mínimos para documentação do sistema, ensaios de comissionamento, inspeção e avaliação de desempenho. Rio de Janeiro: Associação Brasileira de Normas Técnicas (ABNT).

ABSOLAR – Associação Brasileira de Energia Solar Fotovoltaica (2025) Photovoltaic Solar Energy in Brazil. Infographic No. 82. Updated on 12 August 2025.

Almeida, M.P. and Zilles, R. (2012) 'Cálculo de parâmetros de desempenho para sistemas fotovoltaicos conectados à rede', Revista Brasileira de Energia Solar, 3(1), pp. 70–77.

Almeida, M. (2012) Qualification of grid-connected photovoltaic systems. Master's Dissertation. Graduate Program in Energy, University of São Paulo, São Paulo, 171 pp.

Babal, P., Korevaar, M., Franken, S., Mes, J., Bergmans, T. and Wilson, K. (2020) 'Uncertainties in irradiance measurements of sensors to POA rear of bifacial solar panels', in Proceedings of the 47th IEEE Photovoltaic Specialists Conference (PVSC), Calgary, AB, Canada, pp. 959–963. doi: 10.1109/PVSC45281.2020.9301008.

Baratto, A.C., et al. (2008) Avaliação de dados de medição – Uma introdução ao Guia para a expressão de incerteza de medição (GUM 2008). Rio de Janeiro: Instituto Nacional de Metrologia, Qualidade e Tecnologia (INMETRO).

Braid, J.L., Stein, J.S., King, B.H., Raupp, C., Mallineni, J., Robinson, J. and Knapp, S. (n.d.) Effective Irradiance Monitoring Using Reference Modules. Albuquerque, NM: Sandia National Laboratories.

Halliday, D., Resnick, R. and Walker, J. (2014) Fundamentals of physics. 10th edn, Extended. Hoboken, NJ: Wiley.

International Electrotechnical Commission (IEC) (2016a) IEC TS 61724-2: Photovoltaic system performance – Part 2: Power performance index and capacity evaluation method. Geneva: IEC.

International Electrotechnical Commission (IEC) (2016b) IEC TS 61724-3: Photovoltaic system performance – Part 3: Energy evaluation method. Geneva: IEC.

International Electrotechnical Commission (IEC) (2019a) IEC 60904-1-2: Photovoltaic devices – Measurement of current–voltage characteristics of bifacial photovoltaic (PV) devices. Geneva: IEC.

International Electrotechnical Commission (IEC) (2019b) IEC 60904-4: Photovoltaic devices – Procedures for establishing calibration traceability. Geneva: IEC.

International Electrotechnical Commission (IEC) (2021a) IEC 61215-2: Terrestrial photovoltaic (PV) modules – Design qualification and type approval – Part 2: Test procedures. Geneva: IEC.

International Electrotechnical Commission (IEC) (2021b) IEC 61724-1: Photovoltaic system performance – Part 1: Monitoring. Geneva: IEC.

International Electrotechnical Commission (IEC) (2023) IEC 60904-2: Photovoltaic devices – Requirements for photovoltaic reference devices. Geneva: IEC.

International Energy Agency (IEA) (2021) Bifacial photovoltaic modules and systems: Experience and results from international research and pilot applications (Report IEA-PVPS T13-14:2021). Paris: Photovoltaic Power Systems Programme (IEA PVPS).

International Energy Agency (IEA) (2024) Trends in Photovoltaic Applications 2024 (Report IEA-PVPS T1-43:2024). Paris: Photovoltaic Power Systems Programme (IEA PVPS).

International Energy Agency (IEA) (2025) Trends in Photovoltaic Applications 2025 (Report IEA-PVPS T1-48:2025). Paris: Photovoltaic Power Systems Programme (IEA PVPS).

Ledesma, J.R., Almeida, R.H., Martínez-Moreno, F., Rossa, C., Martín-Rueda, J., Narvarte, L. and Lorenzo, E. (2020) 'A simulation model of the irradiation and energy yield of large bifacial photovoltaic plants', Solar Energy, 211, pp. 187–198. https://doi.org/10.1016/j.solener.2020.05.108